Monthly Notices of the ROYAL ASTRONOMICAL SOCIETY

MNRAS **506,** 298–305 (2021) https://doi.org/10.1093/mnras/stab1680
Advance Access publication 2021 June 14

Searching for Saturn's X-rays during a rare Jupiter Magnetotail crossing using *Chandra*

D. M. Weigt [1]★ W. R. Dunn,[2] C. M. Jackman,[3] R. Kraft,[4] G. Branduardi-Raymont,[2] J. D. Nichols,[5] A. D. Wibisono [2] M. F. Vogt[6] and G. R. Gladstone[7,8]

[1]*School of Physics and Astronomy, University of Southampton, Southampton, SO17 1BJ, UK*
[2]*Mullard Space Science Laboratory, Department of Space and Climate Physics, University College London, Dorking, RH5 6NT, UK*
[3]*School of Cosmic Physics, DIAS Dunsink Observatory, Dublin Institute for Advanced Studies, Dublin 15, Dublin, Ireland*
[4]*Harvard–Smithsonian Center for Astrophysics, Smithsonian Astrophysical Observatory, Cambridge, MA 02138, USA*
[5]*Department of Physics and Astronomy, University of Leicester, Leicester, LE1 7RH, UK*
[6]*Center for Space Physics, Boston University, Boston, MA 02215, USA*
[7]*Space Science and Engineering Division, Southwest Research Institute, San Antonio, TX 78238,, USA*
[8]*Department of Physics and Astronomy, University of Texas at San Antonio, San Antonio, TX 78249, USA*

Accepted 2021 June 9. Received 2021 June 4; in original form 2021 April 30

ABSTRACT

Every 19 yr, Saturn passes through Jupiter's 'flapping' magnetotail. Here, we report *Chandra* X-ray observations of Saturn planned to coincide with this rare planetary alignment and to analyse Saturn's magnetospheric response when transitioning to this unique parameter space. We analyse three Director's Discretionary Time (DDT) observations from the High Resolution Camera (HRC-I) on-board *Chandra*, taken on 2020 November 19, 21, and 23 with the aim to find auroral and/or disc emissions. We infer the conditions in the kronian system by looking at coincident soft X-ray solar flux data from the *Geostationary Operational Environmental Satellite* (*GOES*) and *Hubble Space Telescope* (*HST*) observations of Saturn's ultraviolet (UV) auroral emissions. The large Saturn–Sun–Earth angle during this time would mean that most flares from the Earth-facing side of the Sun would not have impacted Saturn. We find no significant detection of Saturn's disc or auroral emissions in any of our observations. We calculate the 3σ upper band energy flux of Saturn during this time to be 0.9–3.04 $\times$ 10^{-14} erg cm^{-2} s^{-1} which agrees with fluxes found from previous modelled spectra of the disc emissions. We conclude by discussing the implications of this non-detection and how it is imperative that the next fleet of X-ray telescope (such as *Athena* and the *Lynx* mission concept) continue to observe Saturn with their improved spatial and spectral resolution and very enhanced sensitivity to help us finally solve the mysteries behind Saturn's apparently elusive X-ray aurora.

Key words: planets and satellites: general – planets and satellites: individual: Saturn – X-rays: individual: Saturn.

1 INTRODUCTION

The magnetospheres of Jupiter and Saturn are considered to be the two largest coherent structures in our Solar system with most of the plasma supplied by their moons and a variable interaction with the upstream solar wind (Blanc et al. 2015; Bolton et al. 2015). The magnetotail of Jupiter is so vast that it extends beyond Saturn's orbit at 9.5 au (on average) (Kurth et al. 1982; Lepping et al. 1982), and contains a wide variety of plasma populations with different structures and velocities (McComas et al. 2007). Lepping et al. (1983) found that Jupiter's magnetotail 'flaps' over a 2–3 day cadence and that the structure and movement of the tail are both determined by the variable solar wind dynamic pressure surrounding the jovian magnetosphere. Both *Voyager* missions found that the tail had a density of $\sim$$10^{-3}$–$10^{-5}$ cm^{-3} (Gurnett, Kurth & Scarf 1979; Lepping et al. 1983; Kurth et al. 1982), several orders of magnitude smaller than the denser, typical solar wind as observed close to Saturn ($\sim$0.01–0.5 cm^{-3}) (Lepping et al. 1983). As a result, the tail is theorized to resemble a 'sausage string' carved by the solar wind with higher dynamic pressure creating the narrower structures of the tail and weaker pressure for the expanded regions. Every $\sim$19–20 yr, the alignment of the gas giants is such that Saturn is located in Jupiter's wake with Saturn's magnetosphere alternately immersed in the solar wind and the rarefied deep jovian magnetotail. This phenomenon of 'overlapping' planetary magnetospheric environments in the Solar system is unique to Jupiter and Saturn due to the sheer scale of the jovian system. The Voyager 2 flyby of Saturn in 1981 occurred during the same planetary alignment which we observe in 2020. At that time, the evidence for the immersion of Saturn in Jupiter's tail came from the radio data, with almost complete dropouts of the Saturn Kilometric Radiation (SKR) observed (Desch 1983). SKR emissions are observed at a frequency range of a few kHz to 1200 kHz on the dawn-noon sector of Saturn's auroral zone (Lamy et al. 2009) and, like other planetary radio emissions (e.g. auroral kilometric radiation at Earth and jovian radio emissions), are believed to be produced from accelerated beams of electrons in the aurora via the cyclotron maser

★ E-mail: D.M.Weigt@soton.ac.uk

instability (Zarka 1998). Further studies into SKR (e.g Reed et al. 2018) found that these emissions can be used as a remote diagnostic tool to infer magnetospheric conditions at Saturn, as the time-scale of many observed SKR events were found to correlate with possible auroral drivers (e.g. changing solar wind dynamic pressure or tail reconnection). Desch (1983) observed during the flyby that the SKR emissions returned to a normal range of intensity when Saturn was back in the solar wind. The dropouts were therefore an indicator of intervals when Saturn was within Jupiter's magnetotail and were used as a tracer for the tail's apparent flapping motion. During this time, no observations of Saturn's auroral emissions in UV or X-ray wavelengths were taken and thus the global context for Saturn's magnetospheric response to such rare external conditions was not fully captured.

The magnetospheric responses of both Jupiter and Saturn to various external (e.g. the solar wind) and internal (e.g. rapid rotation of the planet, moon–planet interactions) drivers (Bagenal 1992) have been studied extensively using auroral measurements in the ultraviolet (UV; e.g. Nichols et al. 2010, 2016), infrared (IR; e.g. Badman et al. 2011), Stallard et al. (2008a, b) and radio (e.g. Kurth et al. 2005; Lamy et al. 2009) wavebands. The processes are found to be highly complex in all wavebands and their auroral responses are varied [see detailed reviews by Bhardwaj & Gladstone (2000) and Badman et al. (2015) for an overview of each of these processes].

Compared to the other wavebands, the drivers of the X-ray auroral emissions remain the most mysterious. Auroral X-ray emissions are postulated to be present on Saturn since the discovery of its magnetosphere by the *Voyager* spacecraft (Opp 1980; Sandel et al. 1982) and the detection of its powerful auroral UV emissions at high latitudes (Broadfoot et al. 1981). The location and spectrum of these UV emissions suggested that they were caused by precipitating electrons with energies of ∼10 s keV (Carbary & Krimigis 1983). Such energetic emissions from electrons would suggest that X-ray bremsstrahlung processes would also be occurring. The first observation to try to detect the X-ray emissions from Saturn was carried out by the *Einstein Observatory* on 1979 December 17 (Gilman et al. 1986), prompted by the discovery of X-ray aurora on Jupiter (Metzger et al. 1983). From the ∼11 ks observation of Saturn, no emissions were detected. Gilman et al. (1986) therefore concluded that bremsstrahlung was likely to be the dominant process for X-ray production. From this assumption, they calculated a 3σ upper limit for the kronian X-ray flux at Earth to be 1.7×10^{-13} erg cm^{-2} s^{-1}. The value is compared with the expected energy flux detected at Earth, using a non-relativistic thick target bremsstrahlung model based on UV observations (Sandel et al. 1982), of 8×10^{-16} erg cm^{-2} s^{-1}. This assumes that the thick-target bremsstrahlung occurs at high latitudes. The first significant detection of Saturn's X-rays was found by *ROSAT* on 1991 April 30 as part of a campaign to observe the gas and ice giants (Uranus and Neptune) (Ness & Schmitt 2000). Ness & Schmitt (2000) found that the upper limits of X-ray luminosites observed from Jupiter were much brighter that what was seen from the other three planets, which were found to have similar levels of weaker X-ray power. *ROSAT* found the X-ray flux of Saturn to be greater than one order of magnitude than the Gilman et al's modelled bremsstrahlung flux. They concluded that this rise in flux may be due to a higher electron flux background that previous observations or an indicator of multiple X-ray mechanisms at Saturn in addition to X-ray bremsstrahlung.

Subsequent X-ray campaigns with *XMM–Newton* on 2002 September 10 (Ness, Schmitt & Robrade 2004a) and *Chandra* on 2003 April 14 (Ness et al. 2004b) discovered that, like Jupiter, Saturn has been observed to produce X-ray emissions from the planetary disc via elastic scattering of solar X-rays from its upper atmosphere. Further *Chandra* observations taken during 2004 January which coincided with an M6-class solar flare found that the disc X-ray flux increased by ∼5 times when the flare impacted Saturn (Bhardwaj et al. 2005b). The scattering mechanisms responsible for the disc emissions would require Saturn's disc to have a high X-ray albedo (Ness et al. 2004b). Bhardwaj et al. (2005c) also found the X-ray spectrum of Saturn's rings was dominated by an atomic oxygen Kα fluorescence line at 0.53 keV, providing evidence for another X-ray mechanism on Saturn. Branduardi-Raymont et al. (2010) re-analyse the previous X-ray campaigns as well as two *XMM–Newton* observations in 2005 and found that Saturn's disc emissions were well correlated with the solar cycle. The results from the Branduardi-Raymont et al. (2010) study verified what was found in previous literature and found the oxygen fluorescence line from the ring region varied differently from the disc emissions. During 2011 April–May, *Chandra* ACIS observations of Saturn were triggered to coincide with the predicted arrival of a solar wind shock, as determined from a propagated solar wind model (Branduardi-Raymont et al. 2013). *In situ Cassini* data during the *Chandra* intervals confirmed the arrival of a solar wind shock at Saturn. Branduardi-Raymont et al. (2013) found X-ray emissions corresponding to scattering of solar X-rays in the upper atmosphere during an episode of flaring activity from the Sun. However, like all previous X-ray campaigns, there was no significant detection of X-ray aurora on Saturn. This led to the conclusion that more powerful solar wind shocks would be required to produce a signal above *Chandra's* threshold of detectability. If shocks are acting on the planet, previous results would suggest that a mechanism producing X-ray bremsstrahlung may exist and are produced in a similar way as observed on Jupiter with photon energies >2 keV (Branduardi-Raymont et al. 2008), known as hard X-rays. These hard X-rays are emitted within the auroral region and have been observed to sometimes coincide with the main UV auroral oval. The brightest and most concentrated emissions are found from soft (<2 keV) X-ray photons which are often concentrated into a hotspot poleward of the main UV oval. The emissions have observed during many X-ray campaigns of Jupiter since their discovery by Gladstone et al. (2002) almost 20 yr ago (e.g. Branduardi-Raymont et al. 2004, 2007a, b), and have been found to exhibit quasi-periodic pulsations (e.g. Dunn et al. 2016; Wibisono et al. 2020; Weigt et al. 2020). Such emissions are produced from charge exchange between precipitating ions, mainly from the volcanic moon Io, and the neutrals in the atmosphere (e.g. Cravens et al. 2003; Elsner et al. 2005; Ozak et al. 2010; Wibisono et al. 2020). There has been no evidence so far of this type of mechanism occurring at Saturn although these emissions, as well as the theorized bremsstrahlung component, may be very dim and below the threshold of detection for both *Chandra* and *XMM–Newton* (Hui et al. 2010).

In this paper, we report the first Chandra Director's Discretionary Time (DDT) observations of Saturn using Chandra's High Resolution Camera (HRC-I) as well as the first X-ray observations specifically designed to look at a planet's magnetospheric response during this rare planetary alignment. We assume that Saturn's magnetosphere will experience more powerful fluctuations as it moves from very rarefied plasma in Jupiter's tail to the denser solar wind (i.e. moving from densities of $\sim 10^{-3}$–10^{-5} cm^{-3} to ∼0.01–0.5 cm^{-3} of the typical solar wind). The *Voyager 2* low density event plasma parameters also found during this time dynamic pressures of $\sim 10^{-4}$ nPa (Lepping et al. 1983), unusually low values compared to the typical observed range of ∼0.01–0.1 nPa (e.g. Jackman & Arridge 2011). These intervals of very low dynamic pressure will cause Saturn's magnetosphere to expand significantly and our study allows us

Table 1. Chandra DDT observations of Saturn throughout 2020 November.

ObsID	Observation Start Date (UT) dd/mm/yyyy	(HH:MM)	Duration (ks)	Apparent diameter	Heliocentric distance (au)	*Chandra*–Saturn distance (au)
24845	19/11/2020	(11:27)	10.0	15.90 arcsec	9.99	10.45
24846	21/11/2020	(12:09)	10.01	15.85 arcsec	9.99	10.48
24847	23/11/2020	(22:44)	9.89	15.80 arcsec	9.99	10.52

to see what effect this dramatic change will have on the kronian magnetosphere. Therefore, the shocks between the solar wind and rarefied tail will be stronger than what typically occurs at Saturn. We also look at data from GOES to monitor the solar activity during each of the observations. We conclude the paper by discussing our results and the implications of a non-detection of Saturn over the *Chandra* campaign and how the next generation of X-ray telescopes could help aid our understanding of Saturn's X-ray emissions.

2 OBSERVATIONS AND DATA ANALYSIS

2.1 *Chandra*

We report the analysis of three ∼10 ks *Chandra* HRC-I X-ray DDT observations of Saturn (ObsID 24845, 24846, and 24847) taken place during 2020 mid-November. The start date, duration, apparent diameter of Saturn, heliocentric and *Chandra*–Saturn distance are shown for each observation in Table 1. The observations were taken in ∼ 2-day cadence to account for the motion of Jupiter's magnetotail, immersing Saturn every 2–3 days (Lepping et al. 1983). All three observations were acquired using *Chandra* HRC-I with the movement of Saturn across the chip corrected for in each observation prior to analysis using the PYTHON equivalent of CIAO's `sso_freeze` algorithm (Weigt et al. 2020).

From previous *Chandra* ACIS and *XMM–Newton* observations of Saturn, disc X-ray emissions have been detected with high statistical significance. The spectrum of the disc emission is well fitted by an optically thin coronal model with average temperature of ∼0.5 keV, resulting from the scattering of solar X-rays in Saturn's upper atmosphere (Branduardi-Raymont et al. 2010). When the fluorescent oxygen emission line found by Bhardwaj et al. (2005b) at 0.53 keV was included in the fit, it was found to significantly improve it. At the time of writing, there have been no statistically significant detections of auroral X-ray photons at Saturn.

The contaminant build-up on ACIS now severly inhibits the detection of X-rays below 1 keV (see Plucinsky et al. 2018), where we expect the peak X-ray photon energy from Saturn to lie. Therefore, these observations were conducted with the High Resolution Camera (HRC). The HRC-I detector on-board *Chandra* has no spectral resolution, resulting in the X-ray photons we analyse being unfiltered into energy bins. This therefore makes it difficult to differentiate between the different possible processes responsible for X-ray production (e.g. bremsstrahlung, solar X-ray scattering) at Saturn. The main focus of these observations, however, was to utilize the high spatial resolution of HRC-I to allow us to separate clearly auroral and disc X-ray regions at Saturn, similar to what can be done at Jupiter. The spatial resolution of HRC-I is ∼ 50% better than that of ACIS allowing us to map any detectable X-ray emissions on to Saturn's surface in greater detail. Once mapped, the intensity of the X-rays is calculated from the 0.8 arcsec full width at half-maximum (FHWM) of the HRC-I point spread function (PSF) as well as the assumptions we consider about the altitude of the emissions in Saturn's ionosphere [more details of the mapping algorithm can be found in Weigt et al. (2020)].

2.2 GOES

To help establish a possible correlation between solar activity and X-ray flux during this time, as found by Bhardwaj et al. (2005b) and Branduardi-Raymont et al. (2010), we use data from the *Geostationary Operational Environmental Satellite* (*GOES*; Lemen et al. 2004). *GOES* is used to monitor the effect weather systems have on Earth as well as space weather effects from the Sun, using instruments such as the *GOES* X-ray Sensor (XRS). We used data from XRS on GOES-16 (Goodman et al. 2013) to monitor any flaring activity from the Sun. The XRS monitors both soft (1–8 Å) and hard (0.5–4 Å) solar X-rays and measures the flux emitted from the Sun. The magnitude of the soft X-ray flux is then used to identify the type of solar flare observed from an A-class (weakest flare: 10^{-8} W m^{-2}) to an X-class flare (strongest flare: $\geq 10^{-4}$ W m^{-2}).

When using the *GOES* data, we take into account the Sun–Earth and Sun–Saturn–Earth light time to ensure we have the correct time for when the radiation from the flare was detected by *GOES* and impacted Saturn, respectively (i.e. as viewed by *Chandra* and *HST*). This was carried out for each of the *Chandra* DDT observations. We also consider the Saturn–Sun–Earth angle during each of the *Chandra* observations. This allows us to get an idea of the direction of any flares found by *GOES*. If this angle is large, the uncertainty of a solar flare found from any detectors near the Earth-facing side of the Sun impacting Saturn will also be large.

3 RESULTS

3.1 *Chandra*

We expect a low-count regime at Saturn based on previous observations. Following Dunn et al. (2021)'s detection of X-rays from Uranus, we divide the detector into a grid of cells the size of the planet. The algorithm first assesses the significance of the detection by splitting the chip into a grid with cells the size of the region of interest i.e. Saturn's disc. Fig. 1 shows the position of Saturn on the chip using the apparent angular diameter of ∼16 arcsec, RA and Dec. from Saturn ephemeris data (JPL Horizons) to create a region using SAOImage DS9 (Joye & Mandel 2003) for ObsID 24847. The region is then overplotted on to the image as shown by the red circle in Fig. 1. The counts within the Saturn region are then compared to the background counts on the remainder of the chip. The X-ray photons shown in Fig. 1 are for ObsID 24847 (2020 November 23) as this observation had the greatest number of counts of the three Saturn observations. The aim-point of the detector is located at the chip centre, surrounded by an error box (navy-dashed 16 arcsec × 12 arcsec box) accounting for possible drifts of the effective aim-point centre. As shown in Fig. 1, the error in the pointing will have a minimal effect on our observations. The PSF of the detector is

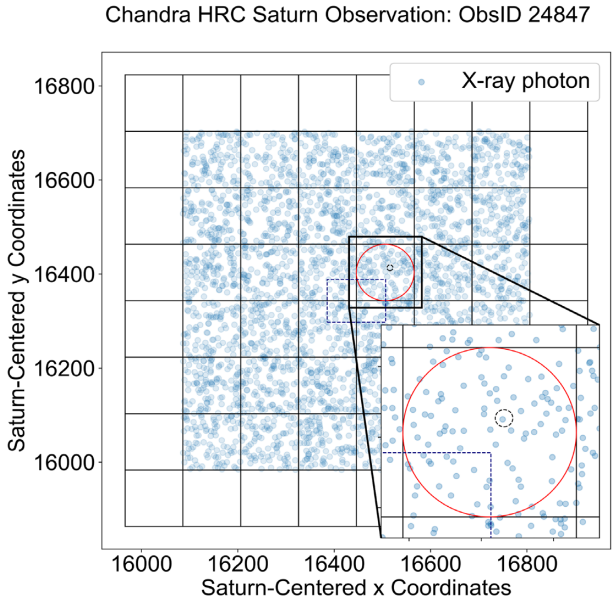

Figure 1. Positions of all X-ray photons (blue dots) on the HRC-I chip, observed during ObsID 24847. The aim-point of the HRC detector is located at the centre of the grid, surrounded by a navy-dashed box (16 arcsec × 12 arcsec) indicating the error associated with the effective aim-point centre. The PSF of the detector is shown by the black-dashed circle. The chip is split into a grid with each box the same width as Saturn's disc during the observation. The corrected position of Saturn on the chip is found to be near the centre, as shown by the red circle. The number of photons in each box are then compared with those found within Saturn to find the significance of the X-ray detection on the disc. Bottom right corner shows the Saturn region in more detail. The position of all photons on the grid has been converted to planetocentric (i.e. Saturn centred) coordinates on the HRC-I chip. The same grid was produced for all three observations.

represented by a black-dashed circle to show our resolution when observing Saturn's disc.

We do not detect Saturn in any of the 2020 November observations. Each of the observations shows no significant detection ($< 3\sigma$ detection from background, where σ is the standard deviation) of auroral or disc X-rays from Saturn during this unique event. The distributions of all counts across the chip within each Saturn-disc sized box (Fig. 1) relative to the counts within the Saturn region for each observation are shown in Fig. 2(a), (c), and (e). Each observation had a similar distribution, with the number of Saturn counts located at the peak of the distribution. This therefore shows that the signal-to-noise ratio was too low for each of the DDT observations and we cannot distinguish Saturn from the background or field of view (FoV) μ. As shown in Table 2 and the histogram distribution of counts in Fig. 2(a), (c), and (e), the mean background or *FoV* counts on the HRC-I chip (*FoV* μ) were comparable to the observed counts found within the Saturn region (C_S: black-dashed line). The total number of boxes across the chip (denoted as N_{Box}) used in the distribution, the *FoV* μ, the percentage of N_{Box} that had fewer counts than C_S and the number of standard deviations C_S is from the *FoV* μ are all displayed in Fig. 2(a), (c), and (e). The total number of Saturn counts and the resulting net counts, $C_S - FoV\ \mu$ for all three observations are displayed in Table 2. Assuming Poissonian statistics and accounting that the kronian X-rays photons are not distinguishable from the background, we calculate the error on the net counts found from ObsID 24847, the observation with the highest C_S, to be 13.71 cts. These assumptions were used for the remaining *Chandra* observations (as shown in Table 2).

We also investigate the time series across the HRC-I chip to search for any time variability in the X-rays registered from the region commensurate with Saturn's position compared to the full distribution. Analysis of similar light curves for Jupiter's X-rays shows features including: disc X-rays that broadly correspond to the solar X-ray activity levels (e.g. Bhardwaj et al. 2005a; Dunn et al. 2020), auroral X-rays that show distinct hotspots in the north and south (e.g. Gladstone et al. 2002; Dunn et al. 2017) as well as quasi-periodic flaring on rare occasions (Jackman et al. 2018; Weigt et al. 2021). For the Saturn case (Fig. 2b, d, and f), the light curve for the entire chip is almost completely flat for all observations, and the subset of this light curve which emerges from the Saturn location is not significant above background.

From the net counts in Table 2, we calculate the 3σ upper limit of the disc emissions during this time. As this is the first auroral observation campaign linked to the alignment of Jupiter and Saturn, this is the first opportunity to predict X-ray powers for this very special case and test them against measurements from previous studies. The true mean for the upper limit is found from the average value of the parameter from the range of net counts for each observation. The energy flux calculation used here assumes a photon energy of ∼0.5 keV, the average temperature of the X-ray emissions found by Branduardi-Raymont et al. (2010), and is an estimate of the flux detected from Saturn. This approach has been used for previous HRC-I observations of Jupiter (Gladstone et al. 2002; Dunn et al. 2017; Weigt et al. 2020, 2021). The upper limit of the emitted disc power was found by multiplying the fluxes by $4\pi\ d^2$, where d is the average geocentric distance of Saturn during each observation. The 3σ upper limit power of the disc from the observation with the highest number of Saturn counts, ObsID 24847, is 0.95 GW, corresponding to an energy flux upper limit of 3.04×10^{-14} erg cm^{-2} s^{-1}, assuming the net counts corresponded to Saturn X-ray emissions. The larger errors in net counts are a result of the high background throughout each observation, mainly from high-energy galactic cosmic ray photons, which are found to exceed or equal the source counts. The upper limits of calculated for all observations are also shown in Table 2.

3.2 Solar data

In the absence of an *in situ* monitor (i.e. a spacecraft in orbit at or near Saturn) we must rely on other remote measurements to infer the conditions in the kronian system at the time of the *Chandra* observations. One way of doing this is through solar observations as we expect, by analogy with Jupiter (Bhardwaj et al. 2005a) and previous X-ray studies of Saturn (Bhardwaj et al. 2005b; Branduardi-Raymont et al. 2010), that the disc power may track the solar X-ray flux as found by *GOES*. The solar soft X-ray flux is found to increase, as well as other wavebands across the electromagnetic spectrum, when the Sun emits a solar flare (Fletcher et al. 2011). In this study, we use the *GOES* solar soft X-ray flux as a diagnostic for solar X-ray activity. The mean *GOES* solar X-ray flux during each observation is shown in Table 2.

To indirectly infer the state of the kronian magnetosphere, one could use auroral observations in other wavelengths. A *Hubble Space Telescope* (*HST*) UV campaign (P.I J. Nichols) has selected observations from 2020 October 29 until November 23, to try and observe the UV auroral response to Saturn being in and out of Jupiter's tail. From this *HST* campaign, there were two *HST* observations within 2 days of the *Chandra* observations on November 22 ∼ 08:20 UT and November 23 ∼ 05:00 UT, ∼18 h before ObsID

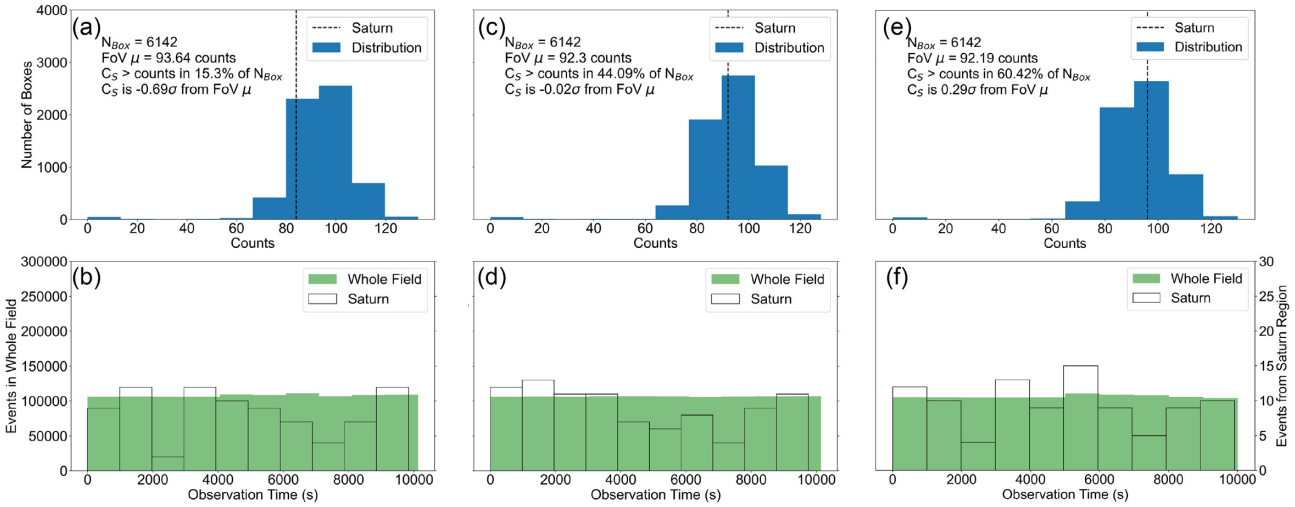

Figure 2. The histogram distribution of counts from each Saturn-disc sized box on the grid (Fig. 1) relative to the number of counts from the Saturn region for (a) ObsID 24845, (c) 24846, and (e) 24847. The corresponding time distributions within the Saturn region (transparent distribution, with *y*-axis on the right) compared to the whole distribution on the chip (green) for all observations are shown in panels (b), (d), and (f), respectively. The counts found from within the Saturn region, C_S, are represented by the black-dashed line in the top panel overlaid on the full count distribution. Shown in text within panel (a) are the total Saturn-disc sized boxes across the detector (N_{Box}), the FoV mean found within the boxes ($FoV\ \mu$) or background counts on the chip, the percentage of N_{Box} that contained a number of counts smaller than C_S and the number of standard deviations (σ) C_S was from the $FoV\ \mu$.

Table 2. *Chandra* DDT observation results from the low count algorithm with upper limit power estimates.

ObsID	Counts in Saturn region (C_S)	Mean background counts ($FoV\ \mu$)	Net counts $\left(\pm\sqrt{(C_S + FoV\ \mu)}\right)$	3σ upper limit[a] disc power (GW)	3σ upper limit[a] disc flux[b]	Mean GOES soft X-ray flux ($\times 10^{-7}$ Wm^{-2})
24845	84	94	-10 ± 13.34	0.28	0.90	0.83
24846	92	92	0 ± 13.56	0.76	2.48	3.17
24847	96	92	4 ± 13.71	0.95	3.04	6.93

[a]Calculated 3σ upper limit as all observations were non-detections.
[b]Upper limit of X-ray disc flux has units $\times\ 10^{-14}$ erg cm^{-2} s^{-1}.

24847. These observations may indicate that the dominant process producing the UV aurora was different between both observations with a dramatic change of morphology from a spiral-like structure to more localized brightening near the pole surrounded by half the UV oval (discussed in more detail in Nichols et al., in preparation). This change in auroral morphology may suggest that the magnetosphere was changing state over short time-scales.

The soft X-ray flux from *GOES* and the observation intervals of both *HST* (dashed black lines) and the three *Chandra* observations (shaded orange regions) are shown in Fig. 3 for the entire month of November (panel a) and the week encompassing the *Chandra* observations (panel b). We note that there was no *GOES* 16 data from November 5 until November 16. As shown in Fig. 3, the *GOES* solar soft X-ray flux was found to increase from around November 20 and plateau at an overall higher average solar flux from November 23. This is also shown in Table 2 with the increase in mean solar X-ray flux throughout the *Chandra* campaign. This flux level is then observed to be maintained throughout the remainder of the month (Fig. 3b). The solar flux during our observations indicates a possible C-class flare coinciding with or arriving at Saturn just before ObsID 24847. The Sun–Earth and Sun–Saturn–Earth light times were used to correct for the *GOES* detection of the flare (light time (*lt*) ∼8.2 min) and for when the flare would impact Saturn as viewed by *Chandra* and *HST* (*lt* ∼ 170 min) and used in all intervals shown in both panels. However, the Saturn–Sun–Earth angles throughout the campaign were found to be ∼72°–89°, suggesting that any flares found from *GOES* would unlikely to have impacted Saturn. The flux of the flare is ∼4×10^{-6} W m^{-2} and, although unlikely to have arrived at Saturn, is found to raise the mean solar flux for the remainder of the campaign. As observed on Jupiter and from previous studies of Saturn, not all of the incident solar photons will be scattered back due to the planet's X-ray albedo (Bhardwaj et al. 2005a; Ness et al. 2004a, b). The X-ray albedo of Saturn is predicted to be $>5.7 \times 10^{-4}$ (slightly higher than Jupiter's at ∼5×10^{-4}) which means that Saturn's upper atmosphere acts like a slightly opaque, diffuse mirror for the incoming solar X-rays, scattering back ∼1 in a few thousand photons. This would allow Saturn to be observed in the soft X-ray energy range, as found previously, and one would expect the increase in solar flux should allow a significant detection of these emissions.

4 DISCUSSION AND CONCLUSIONS

As we have discussed, the first *Chandra* HRC-I DDT observations of X-rays from Saturn during this unique alignment with Jupiter show a non-detection of Saturn (both disc and auroral emissions). We note that the observations occurred during the early rising phase of the solar cycle, when the Sun displays generally low solar X-ray flux, sporadic flaring, and is ejecting short scale fast solar wind streams (e.g. Ataç & Özgüç 2001; Burlaga et al. 2001; Xystouris, Sigala & Mavromichalaki 2014). The solar flux during the DDT campaign only peaked above 10^{-6} W m^{-2} during one of the three observation windows (ObsID 24847) (Fig. 3), immediately after a C-class flare. Due to low solar X-ray fluxes and the large Saturn–Sun–Earth angle

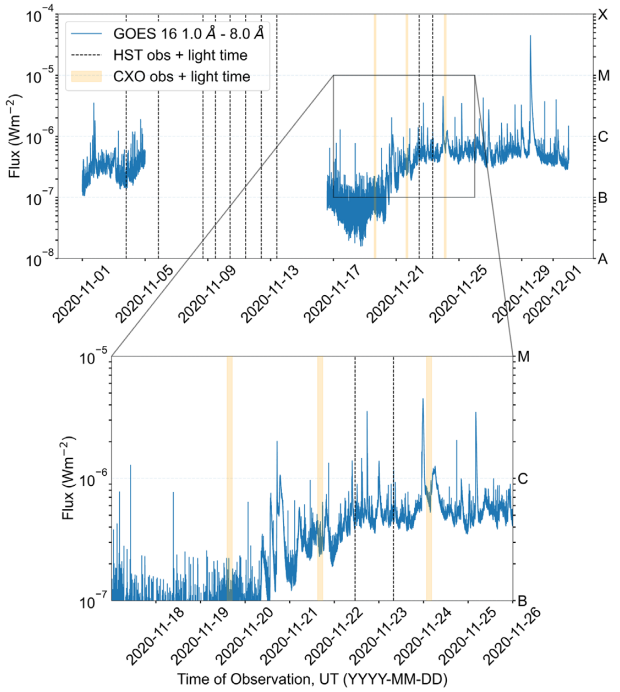

Figure 3. Plots of the observation time versus soft solar X-ray flux in logspace from *GOES* 16 for (a) the full month of November and (b) the week encompassing the *Chandra* observations. There was no *GOES* data recorded between November 5 and November 16. Both *HST* (black dashed line) and *Chandra* (shaded orange regions) observation intervals are plotted in each panel. The Sun–Earth and Sun–Saturn–Earth light times were used to account for the flare being observed by *GOES* and when it impacted Saturn and viewed by *Chandra* and *HST*, respectively. The ObsID 24847 observation window is shown in both panels by the final shaded area. The estimated arrival time of the radiation from the C-class flare is found to impact Saturn just prior to or coincide with ObsID 24847 as shown in both panels. The C-class flare is found to have a flux of $\sim 4 \times 10^{-6}$ W m^{-2}. This is the peak solar flux observed during throughout the *Chandra* campaign after a steady increase of average solar flux throughout November (panel a).

throughout we would expect the disc emissions to be very dim as there will be fewer solar photons undergoing elastic scattering in Saturn's upper atmosphere. This would therefore explain the non-detection of Saturn's disc amongst the background (dominated by high energy galactic cosmic rays) of the chip. We do note, however, that the observation found to have the most Saturn counts (C_S), ObsID 24847, is found to have the highest observed mean *GOES* flux. This agrees with previous studies that have found a similar correlation between the number of disc X-ray photons and solar X-ray flux (e.g. Bhardwaj et al. 2005b).

The calculated 3σ range of upper limit disc energy flux in this study ($0.90–3.04 \times 10^{-14}$ erg cm^{-2} s^{-1}), using our assumptions, is found to be within the upper end of the range of energy fluxes from modelled spectra of the *Chandra* disc emissions between 0.2 and 2 keV found by Branduardi-Raymont et al. (2010) ($\sim 0.30–1.00 \times 10^{-14}$ erg cm^{-2} s^{-1}). These observations were found to coincide with *GOES* soft X-ray flux measurements exceeding 10^{-6} W m^{-2}, similar to the solar activity measured during 2020 November. Our energy flux upper limits are an order of magnitude less than the 3σ upper limit flux calculated by Gilman et al. (1986) for high latitude, non-relativistic thick-target bremsstrahlung at 1.7×10^{-13} erg cm^{-2} s^{-1}, from their $\sim$11-ks observation. When compared to the results of Ness & Schmitt (2000), our 3σ upper limit flux range lies within both their observed Saturn soft X-ray flux (1.9×10^{-14} erg cm^{-2} s^{-1}) and 95% confidence upper limit flux for hard X-ray flux (1.3×10^{-14} erg cm^{-2} s^{-1}). Therefore our predicted fluxes are consistent with previous observations and predictions. We note that unlike previous *Chandra* observations, no spectra were taken and therefore no energy filtering was carried out for the DDT observations. The estimated power calculated here will therefore include photon energies exceeding the 2 keV upper energy bound of the models used by Branduardi-Raymont et al. (2010). We therefore suggest that future campaigns look again at Saturn during this rare planetary alignment with the next fleet of X-ray telescopes with greatly improved X-ray sensitivity such as *Athena* (Barret et al. 2016) and *Lynx* (Gaskin et al. 2019), one of the mission concepts currently under review for the 2020 Astrophysics Decadal Survey. The collecting area at 1 keV of both *Athena* ($\sim$1.5 m^2) and *Lynx* ($\sim$2.3 m^2) is $\sim$20–30 times greater than *Chandra* ($\sim$0.08 m^2) which allows for deeper exploration of space by increase the limit of detection of fainter sources (assuming a relatively low background). The combination of the large collecting area of *Lynx* with a high spatial resolution (<0.5 arcsec) will allow us to map the fainter individual X-ray photons in greater detail. Although the spatial resolution of *Athena* ($\sim$5 arcsec) is insufficient to allow detailed mapping of the X-ray emissions, the spectral resolution of *Athena's X-ray Integral Field Unit (X-IFU)* is $\sim$2.5 eV up to energies of 7 keV (Barret et al. 2016), surpassing both the *High Definition X-ray Imager* on board *Lynx* ($\sim$70–150 eV at energies 0.3–5.9 keV) and ACIS ($\sim$130–280 eV at energies 1.49–5.9 keV) (Falcone et al. 2019). The high-energy resolution of *Athena* will allow us to find more detailed spectra of the X-ray emissions at Saturn as well as that of the other planets. With the greater sensitivity and spectral resolution of the new X-ray fleet, we would have the capabilities of conducting a deeper search for X-ray aurorae on Saturn. This will allow us to further constrain the disc power and to provide a more accurate estimate of Saturn's disc response to such conditions as well as other planets, further aiding our understanding of the X-ray production mechanisms within our Solar system. However, to ensure we get a significant number of kronian X-ray photons (and planets producing fainter X-ray emissions) to utilize the spectral and spatial capabilities of these telescopes, future observations will need to optimize the exposure time required.

As stated previously, this complicated interaction between two large and complex magnetic environments only occurs between the two gas giants. This was first observed by Voyager 2–40 yr ago during its flyby of Saturn (e.g Desch 1983; Kurth et al. 1982; Lepping et al. 1982, 1983) but no direct auroral measurements were taken. The idea behind our observations was to find whether the shocks produced from Saturn moving from rarefied plasma in Jupiter's magnetotail to the denser solar wind environment would be enough to dramatically compress Saturn's magnetosphere beyond the typical parameter space when Saturn is transitioning from one solar wind regime to another. Within Saturn's magnetosphere, the planetary plasma is dominated by heavy ions in (mainly H_2O^+, OH^+, O^+ produced from Saturn's icy moon Enceladus) (Hui et al. 2010). This campaign afforded us to the opportunity to explore the extremes of parameter space at Saturn, and crucially the change between the typical water-rich kronian magnetosphere immersed in a variable solar wind, to a magnetosphere immersed in the rarefied jovian magnetotail. With the non-detection of Saturn throughout each of the observations, our analysis suggests that even with such a variable external driver, the dramatic compressions are still not enough to energize the heavy ions and produce X-ray aurorae. As stated by Hui et al. (2010), another likely possibility is that the field potentials at

Saturn are too low to sufficiently charge strip magnetospheric plasma or to increase solar wind ion fluxes sufficiently to generate observable X-ray ion aurora (Cravens et al. 2003; Clark et al. 2020).

From inspection of the two *HST* observations taken within 2 days before ObsID 24847, a spiral-like morphology in the UV auroral oval is observed on November 22 and a more localized brightening near the pole is found hours before the *Chandra* observation. Models of the spiral morphology suggest that it is created from precipitation of hot plasma during intervals of steady yet unbalanced rapid reconnection in Saturn's magnetotail and during dayside magnetic reconnection (Cowley, Bunce & O'Rourke 2004; Jackman et al. 2004). This latter type of reconnection may be associated with a shock, compressing the magnetosphere [e.g. possible shocks from the solar wind (Badman et al. 2016)] and is more likely to vary with solar wind dynamic pressure. One possible cause of the localized polar auroral brightening is from a dawn storm, auroral emissions from compression induced magnetic reconnection in Saturn's magnetotail (Cowley et al. 2005). Unfortunately without a significant X-ray detection during this time, we cannot determine whether there was any unusual X-ray emissions near the pole associated with the UV polar emissions.

This is the first X-ray campaign of its kind to look at a planet's magnetospheric response during such extreme conditions. We hope this work sets the foundations for further exploration into this rare planetary alignment in ∼20 yr time with a new fleet of X-ray telescopes with greater spectral resolution from the *X-IFU* on *Athena* and *Lynx's HDXI*. This will allow tighter observational constraints on the auroral luminosity in all types of environments and add new insight into Saturn's magnetospheric response. This will aid us to solve the mystery behind Saturn's absent X-ray aurora.

ACKNOWLEDGEMENTS

We greatly thank Patrick Slane and the Chandra Scheduling Team for awarding us the Director's Discretionary Time and helping us to set up these unique observations. DMW would like to thank Sophie Murray for discussions on flaring activity during the early rising phase of the solar cycle and retrieving the Geostationary Operational Enviornment Satellite (GOES) data used here. DMW would also like to thank Seán McEntee for discussions on solar X-ray scattering from the upper atmosphere of the gas giants. DMW is supported by the Science and Technology Facilities Council (STFC) studentship ST/S505703/1 and long term attachment grant to work at the Dublin Institute for Advanced Studies (DIAS). WRD was supported by an STFC research grant to University College London (UCL). CMJ's work is supported by the Science foundation Ireland Grant 18/FRL/6199. ADW is supported by STFC studentship ST/S50578X/1. WRD and GB-R acknowledge support from STFC consolidated grant ST/S000240/1 to University College London (UCL).

DATA AVAILABILITY

The Saturn X-ray observations we present here are publicly available from the *Chandra Data Archive* (https://cda.harvard.edu/chaser/). The *GOES* data are publicly available from the National Centers for Enviornmental Information (NCEI) (formely known as National Geophysical Data Center (NGDC)) archives (https://www.ngdc.noaa.gov/stp/satellite/goes-r.html) and can be retrieved and analysed via SUNPY (https://docs.sunpy.org/en/stable/whatsnew/2.1.html#overview).

REFERENCES

Ataç T., Özgüç A., 2001, Solar Phys., 198, 399
Badman S. V. et al., 2011, Icarus, 216, 367
Badman S. V., Branduardi-Raymont G., Galand M., Hess S. L. G., Krupp N., Lamy L., Melin H., Tao C., 2015, Space Sci. Rev., 187, 99
Badman S. V. et al., 2016, Icarus, 263, 83
Bagenal F., 1992, Annu. Rev. Earth. Planet. Sci., 20, 289
Barret D. et al., 2016, in den Herder J.-W. A., Takahashi T., Bautz M., eds, Proc. SPIE Conf. Ser. Vol. 9905, Space Telescopes and Instrumentation 2016: Ultraviolet to Gamma Ray. SPIE, Bellingham, p. 99052F
Bhardwaj A., Gladstone G. R., 2000, Rev. Geophys., 38, 295
Bhardwaj A. et al., 2005a, Geophys. Res. Lett., 32, 1
Bhardwaj A., Elsner R. F., Waite J. H. Jr, Gladstone G. R., Cravens T. E., Ford P. G., 2005b, ApJ, 624, L121
Bhardwaj A., Elsner R. F., Waite J. H. Jr, Gladstone G. R., Cravens T. E., Ford P. G., 2005c, ApJ, 627, L73
Blanc M. et al., 2015, Space Sci. Rev., 192, 237
Bolton S. J. et al., 2015, Space Sci. Rev., 192, 192
Branduardi-Raymont G., Elsner R. F., Gladstone G. R., Ramsay G., Rodriguez P., Soria R., Waite J. H., 2004, A&A, 337, 331
Branduardi-Raymont G. et al., 2007a, Planet. Space. Sci., 55, 1126
Branduardi-Raymont G. et al., 2007b, A&A, 463, 761
Branduardi-Raymont G., Elsner R. F., Galand M., Grodent D., Cravens T. E., Ford P., Gladstone G. R., Waite J. H., 2008, J. Geophys. Res.: Space Phys., 113, 1
Branduardi-Raymont G., Bhardwaj A., Elsner R. F., Rodriguez P., 2010, A&A, 510, 1
Branduardi-Raymont G. et al., 2013, J. Geophys. Res.: Space Phys., 118, 2145
Broadfoot A. L. et al., 1981, Science, 212, 206
Burlaga L. F., Skoug R. M., Smith C. W., Webb D. F., Zurbuchen T. H., Reinard A., 2001, J. Geophys. Res.: Space Phys., 106, 20957
Carbary J. F., Krimigis S. M., 1983, J. Geophys. Res., 88, 8947
Clark G. et al., 2020, J. Geophys. Res.: Space Phys., 125, 1
Cowley S. W. H., Bunce E. J., O'Rourke J. M., 2004, J. Geophys. Res.: Space Phys., 109, A05212
Cowley S. W. et al., 2005, J. Geophys. Res.: Space Phys., 110, 1
Cravens T. E., Waite J. H., Gombosi T. I., Lugaz N., Gladstone G. R., Mauk B. H., MacDowall R. J., 2003, J. Geophys. Res.: Space Phys., 108, 1
Desch M. D., 1983, J. Geophys. Res., 88, 6904
Dunn W. R. et al., 2016, J. Geophys. Res. A.: Space Phys., 121, 2274
Dunn W. R. et al., 2017, Nat. Astron., 1, 758
Dunn W. R. et al., 2020, J. Geophys. Res.: Space Phys., 125, e2019JA027219
Dunn W. R. et al., 2021, J. Geophys. Res.: Space Phys., 126, e2020JA028739
Elsner R. F. et al., 2005, J. Geophys. Res.: Space Phys., 110, 1
Falcone A. D., Kraft R. P., Bautz M. W., Gaskin J. A., Mulqueen J. A., Swartz D. A., 2019, J. Astron. Telesc. Instrum. Syst., 5, 021019
Fletcher L. et al., 2011, Space Sci. Rev., 159, 19
Gaskin J. A. et al., 2019, J. Astron. Telesc. Instrum. Syst., 5, 1
Gilman D. A., Hurley K. C., Seward F. D., Schnopper H. W., Sullivan J. D., Metzger A. E., 1986, ApJ, 300, 453
Gladstone G. R. et al., 2002, Nature, 415, 1000
Goodman S. J. et al., 2013, Atmos. Res., 125, 34
Gurnett D. A. KURTH W. S. SCARF F. L., 1979, Science, 206, 987
Hui Y., Cravens T. E., Ozak N., Schultz D. R., 2010, J. Geophys. Res.: Space Phys., 115, A10239
Jackman C. M., Arridge C. S., 2011, Solar Phys., 274, 481
Jackman C. M., Achilleos N., Bunce E. J., Cowley S. W., Dougherty M. K., Jones G. H., Milan S. E., Smith E. J., 2004, J. Geophys. Res.: Space Phys., 109, A11203
Jackman C. M. et al., 2018, J. Geophys. Res.: Space Phys., 123, 9204
Joye W., Mandel E., 2003, ASP Conf. Ser. Vol. 295, Astronomical Data Analysis Software and Systems XII. Astron. Soc. Pac., San Francisco, p. 489
Kurth W. S., Sullivan J. D., Gurnett D. A., Scarf F. L., Bridge H. S., Sittler E. C., 1982, J. Geophys. Res., 87, 10373
Kurth W. S. et al., 2005, Nature, 433, 722

Lamy L., Cecconi B., Prangé R., Zarka P., Nichols J. D., Clarke J. T., 2009, J. Geophys. Res.: Space Phys., 114, 1
Lemen J. R. et al., 2004, inFineschi S. , Gummin M., eds, Proc. SPIE Conf. Ser. Vol. 5171, Telescopes and Instrumentation for Solar Astrophysics.SPIE, Bellingham, p. 65
Lepping R. P., Burlaga L. F., Desch M. D., Klein L. W., 1982, Geophys. Res. Lett., 9, 885
Lepping R. P., Desch M. D., Klein L. W., Sittler E. C., Sullivan J. D., Kurth W. S., Behannon K. W., 1983, J. Geophys. Res.: Space Phys., 88, 8801
McComas D. J., Allegrini F., Bagenal F., Crary F., Ebert R. W., Elliott H., Stern A., Valek P., 2007, Science, 318, 217
Metzger A. E., Gilman D. A., Luthey J. L., Hurley K. C., Schnopper H. W., Seward F. D., Sullivan J. D., 1983, J. Geophys. Res., 88, 7731
Ness J. U., Schmitt J. H., 2000, A&A, 355, 394
Ness J. U., Schmitt J. H., Robrade J., 2004a, A&A, 414, 49
Ness J. U., Schmitt J. H., Wolk S. J., Dennerl K., Burwitz V., 2004b, A&A, 418, 337
Nichols J. D. et al., 2010, Geophys. Res. Lett., 37, 1
Nichols J. D., Badman S. V., Bunce E. J., Clarke J. T., Cowley S. W., Hunt G. J., Provan G., 2016, Icarus, 263, 17
Opp A. G., 1980, Science, 207, 401
Ozak N., Schultz D. R., Cravens T. E., Kharchenko V., Hui Y. W., 2010, J. Geophys. Res.: Space Phys., 115, 1
Plucinsky P. P., Bogdan A., Marshall H. L., Tice N. W., 2018, in den Herder J.-W. A., Nikzad S., Nakazawa K., eds, Proc. SPIE Conf. Ser. Vol. 10699, Space Telescopes and Instrumentation 2018: Ultraviolet to Gamma Ray. SPIE, Bellingham, p. 106996B
Reed J. J., Jackman C. M., Lamy L., Kurth W. S., Whiter D. K., 2018, J. Geophys. Res.: Space Phys., 123, 443
Sandel B. R. et al., 1982, Science, 215, 548
Stallard T., Miller S., Melin H., Lystrup M., Cowley S. W. H., Bunce E. J., Achilleos N., Dougherty M., 2008a, Nature, 453, 1083
Stallard T. et al., 2008b, Nature, 456, 214
Weigt D. M. et al., 2020, J. Geophys. Res.: Planets, 125, e2019JE006262
Weigt D. M., Jackman C. M., Vogt M. F., Manners H., Dunn W. R., Gladstone G. R., Kraft R., Branduardi-raymont G., 2021, Characteristics of Jupiter's X-ray auroral hot spot emissions using Chandra [preprint], https://essoar.org, doi: 10.1002/essoar.10506198.1
Wibisono A. D. et al., 2020, J. Geophys. Res.: Space Phys., 125, e2019JA027676
Xystouris G., Sigala E., Mavromichalaki H., 2014, Solar Phys., 289, 995
Zarka P., 1998, J. Geophys. Res.: Planets, 103, 20159

This paper has been typeset from a TEX/LATEX file prepared by the author.